

Raman imaging to investigate ultrastructure and composition of plant cell walls: distribution of lignin and cellulose in black spruce wood (*Picea mariana*)

Umesh P. Agarwal

Received: 30 January 2006 / Accepted: 14 April 2006 / Published online: 8 June 2006
© Springer-Verlag 2006

Abstract A detailed understanding of the structural organization of the cell wall of vascular plants is important from both the perspectives of plant biology and chemistry and of commercial utilization. A state-of-the-art 633-nm laser-based confocal Raman microscope was used to determine the distribution of cell wall components in the cross section of black spruce wood in situ. Chemical information from morphologically distinct cell wall regions was obtained and Raman images of lignin and cellulose spatial distribution were generated. While cell corner (CC) lignin concentration was the highest on average, lignin concentration in compound middle lamella (CmL) was not significantly different from that in secondary wall (S2 and S2–S3). Images generated using the $1,650\text{ cm}^{-1}$ band showed that coniferaldehyde and coniferyl alcohol distribution followed that of lignin and no particular cell wall layer/region was therefore enriched in the ethylenic residue. In contrast, cellulose distribution showed the opposite pattern—low concentration in CC and CmL and high in S2 regions. Nevertheless, cellulose concentration varied significantly in some areas, and concentrations of both lignin and cellulose were high in other areas.

Though intensity maps of lignin and cellulose distributions are currently interpreted solely in terms of concentration differences, the effect of orientation needs to be carefully considered to reveal the organization of the wood cell wall.

Keywords Black spruce · Cell wall · Cellulose · Lignin · Microscopy · Raman imaging

Introduction

The plant cell wall is a heterogeneous natural nanocomposite of cellulose, lignin, and hemicelluloses (Fengel and Wegner 1984). The cell wall also contains small amounts of pectin and protein in some areas. Cellulose, the major component of the cell wall, is a polysaccharide made up of (1 → 4)- β -D-glucopyranose units. In wood, it is 50–60% crystalline (Newman 2004) and is assembled from nano-fibrils (traditionally called cellulose microfibrils) to provide a rigid reinforcing layer around the cell membranes in plants. Lignin, the second most abundant polymer in plants, consists of phenyl propane units and plays an important supportive role. Lignin is made by condensation reactions between three major structural units: coumaryl, coniferyl, and sinapyl alcohols. After cellulose, hemicelluloses constitute the most abundant group of carbohydrates in plant cell walls. Hemicelluloses are branched polymers made up of several monosaccharides. Hemicelluloses and lignin provide the matrix in which cellulose nano-fibrils are extensively cross-linked to hemicellulose polysaccharide chains.

The cell wall is organized in several layers (Fig. 1). The primary wall (P), secondary wall (S1, S2, and S3),

The Forest Products Laboratory is maintained in cooperation with the University of Wisconsin. This article was written and prepared by U.S. Government employees on official time, and it is therefore in the public domain and not subject to copyright. The use of trade or firm names in this publication is for reader information and does not imply endorsement by the U.S. Department of Agriculture of any product or service.

U. P. Agarwal (✉)
Forest Products Laboratory, USDA Forest Service,
One Gifford Pinchot Drive, Madison, WI 53726, USA
e-mail: uagarwal@fs.fed.us

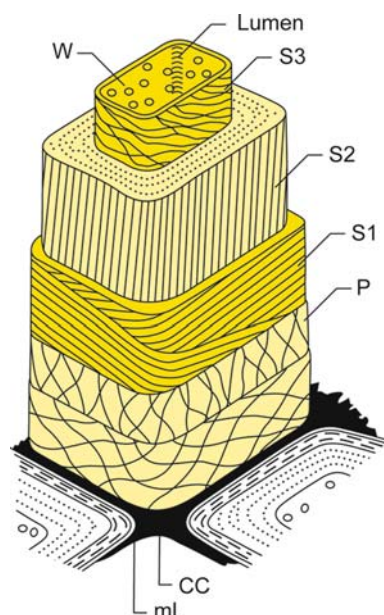


Fig. 1 Schematic depiction of tracheid cell wall structure in black spruce wood: *W* thin warty layer in cell lumen; *S3*, *S2*, *S1* secondary wall layers; *P*, *mL* primary wall and middle lamella, respectively; *CC* cell corner middle lamella. Layer thickness is *S3*, ~ 0.1 μm ; *S2*, 1–5 μm ; *S1*, 0.2–0.3 μm ; *P*, 0.1–0.2 μm ; *mL*, 0.2–1.0 μm . *Parallel* and *wavy lines* indicate different organization of cellulose nano-fibrils (Sjostrom 1993)

and middle lamella (*mL*) have different structures. Likewise, within the secondary wall, *S1*, *S2*, and *S3* differ with respect to the orientation of cellulose nano-fibrils. The middle lamella surrounds the cell and holds the neighboring cells together. An understanding of cell wall architecture is important for both research and technological purposes. Basic information is needed to comprehend how growth and development factors influence cell wall formation. For example, such information will be useful for understanding how the cell wall structure is modified in response to environmental stimuli. Additionally, from the technological perspective, structural insights are important to understand the mechanical, chemical, and biological behaviors of plants and plant materials. A better structural understanding of wood, for instance, will lead to an improved understanding of wood-based materials (Åkerholm and Salmén 2003; Ehrnrooth et al. 1984; Green et al. 1999; Olsson and Salmén 1997; Salmén and Olsson 1998). Moreover, it will help in addressing the question of how different chemical, biological, and mechanical processing of wood can lead to materials with superior properties.

Several techniques have been applied to the study of subcellular distribution and organization of wood components (Daniel et al. 1991; Donaldson and Ryan 1987; Eriksson et al. 1988; Fergus et al. 1969; Imai and

Terashima 1992; Parameswaran and Liese 1982; Peng 1997; Saka and Goring 1988; Scott et al. 1969; Tirumalai et al. 1996; Westermark et al. 1988). Cellulose has been more difficult to analyze than lignin. A number of traditional methods require isolation of morphologically distinct tissue or sectioning of tissue by embedding the samples. Such methods are enormously disruptive to native-state structures. Moreover, methods such as optical and electron microscopy describe only cell wall morphology and do not provide information on molecular structure. Additionally, for lignin analysis using electron microscopy–energy dispersive X-ray analysis (EM–EDXA), chemical treatment by Br_2 or Hg is indicated (Donaldson and Ryan 1987; Westermark et al. 1988). None of these limitations exists in Raman imaging because sampling is done directly. Besides, both lignin and cellulose can be mapped simultaneously by selecting Raman bands that are specific to these cell wall components. The intent of the work presented here is to develop a Raman imaging methodology for mapping woody tissues and generate information on the organization and distribution of the constituent polymers in various cell wall layers.

Raman microscopy was previously used to analyze cell walls in situ; the research showed that information on both cellulose and lignin can be obtained (Agarwal and Atalla 1986; Atalla and Agarwal 1985; Bond and Atalla 1999; Tirumalai et al. 1996). However, at that time progress towards detailed cell wall investigations was hindered due to the limitations driven by both sampling and instrumentation. Sample fluorescence and a lignin band that was less than fully stable made Raman investigations difficult. In addition, a highly efficient Raman microprobe equipped with an automated high-resolution *x*, *y* stage was not available.

In the 1990s, new technologies like the holographic notch filter and the availability of charge-coupled devices (CCD) that acted as multichannel detectors decreased acquisition time by more than an order of magnitude (Baldwin et al. 2002). Rugged, air-cooled lasers (e.g., He–Ne 633 nm) simplified utility requirements and provided more beam-pointing stability compared with that of water-cooled lasers. Furthermore, sampling in confocal mode reduced fluorescence by physically blocking the signal originating from the volume of the sample not in focus. The detected Raman signal came from the illuminated spot.

The latest Raman microprobes incorporate these advances and are well suited to investigate lignin and cellulose distribution in the cell walls of woody tissue. These capabilities permit compositional mapping of the woody tissue with chosen lateral and axial spatial resolutions. Thousands of spectra can now be obtained

in a realistic time frame to generate component-specific Raman images for studying wood ultrastructure. A 785-nm near-IR laser-based Raman system was recently applied to the study of beech cell walls (Roder et al. 2004). Here, our objective is to show that a higher resolution, 633-nm, visible, laser-based confocal Raman microprobe can be used to investigate the plant cell wall in detail; specifically, the ultrastructural compositional heterogeneity of the cell wall in a cross-section of black spruce.

Experimental

Sample preparation

A 55- to 57-year-old black spruce [*P. mariana* (Miller) B.S.P.] tree was harvested from northern Wisconsin. The samples were taken from the main stem and no compression wood was present in the area of the samples. Transverse sections, 1 cm by 0.5 cm by 10 μm thick, were prepared by microtome from segments between the 30th and 40th annual rings. Five transverse sections taken from these annual ring segments were studied. The sections were stored in 95% ethanol. Prior to sampling, the selected section was sequentially extracted with acetone:water (9:1), toluene:ethanol (2:1), and methanol. The extracted section was air dried under a no. 1 glass coverslip and affixed to one side of a double-stick carbon tape disc. Prior to adhering the section, a hole was punched through the center of the disc so that light could pass through and the section could be imaged in bright field. The other side of the disc was fixed to a microscopic glass slide.

Raman analysis

A Raman microprobe spectrometer, LabRam HR 800 (Horiba Jobin Yvon, Edison, NJ, USA) was used in the present study. This spectrometer is equipped with a confocal microscope (Olympus BX40), a piezoelectric x , y stage, and a CCD detector. This instrument provides ultra-high spectroscopic resolution and unique polarized 633-nm laser (20-mW) excitation, which capacitates the system for woody tissue investigations. Woody tissue spectra from various morphological regions were obtained by using the serial (raster) mapping technique (Fig. 2). Woody tissue was placed on an automated piezoelectric x , y mapping stage, and Raman spectra were obtained at different points in the tissue by moving it equivalently under the microscopic objective. For mapping in the x , y plane at chosen spatial resolutions, the specimen was moved in the two

spatial dimensions (x and y) and a spectrum was recorded at each (x , y) position. The vertical z displacement was controlled with the manual micrometer adjustment; in the present case, only the surface of the woody tissue was sampled. The electric vector of the laser was in the x direction. Since the x , y stage was not a rotating stage, sample rotation was not possible. The spectral and spatial information was recorded using a two-dimensional CCD detector. Laser power was measured both before and after the experiment and remained constant. The operating parameters for the LabRam HR 800 were kept constant for all measurements. The spectrum from each location was obtained by averaging two 15-s cycles. A minimum of two cycles was needed by the instrument software to remove the cosmic spikes from the spectrum. This also improved the signal-to-noise ratio.

An Olympus 100X MPlan metallurgical objective, NA 0.90, was used for the Raman studies. Different acquisition times were used depending on the signal-to-noise ratio desired and the duration of the experiment. Similarly, experiments with different spatial resolutions were carried out depending on the nature of the information desired. Confocal aperture was set at 100 μm for all experiments. The reported depth resolution for the 100- μm confocal hole, based on the silicon (standard) phonon band at 520 cm^{-1} , was $\sim 4 \mu\text{m}$. The lateral resolution of the confocal Raman microscope was $\sim 1 \mu\text{m}$. This was supported by the Raman imaging (see Fig. 6a), where 1 μm CC and mL regions could be discretely visualized. The lateral resolution was significantly lower than the theoretical prediction ($0.61 \lambda/\text{NA}$, Bradbury 1989), where λ is the wavelength of the laser and NA is the numerical aperture of the microscopic objective. Considering the lateral resolution, only the S2 and CC areas of the distinct cell wall regions (Fig. 1) could be sampled by themselves. Other investigated areas had contributions from two or more layers. For example, sampling in the mL region incorporated the P walls of the adjoining cells (mL + P, called the CmL region), but there also may have been some contribution from S1 depending on the thickness of the CmL region. For the purposes of the present study, the total mapped area was analyzed in terms of the CC, CmL, S2, S2–S3, and lumen regions. LabSpec 4.02 software was used to obtain Raman spectra in specific spectral ranges (250–3,200 cm^{-1}). This software was used to perform all spectrometer operations, process collected data, and generate Raman images. Such images were based on component-specific spectral regions and represented distribution of the cell wall components. Unless stated otherwise, Raman band regions 1,519–1,712 and

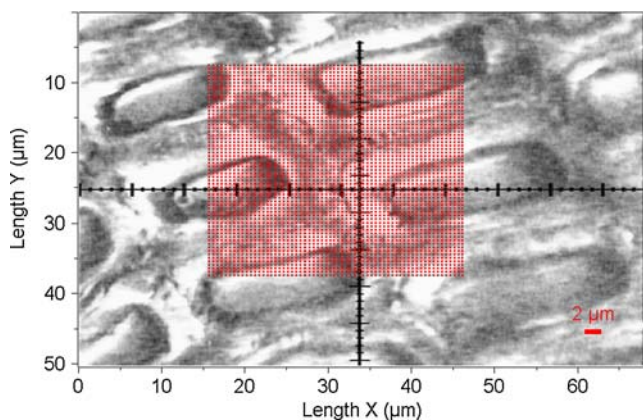


Fig. 2 Bright field (*white light*) image of woody tissue with superimposed sampling grid pattern (30 by 30 μm at 0.5 μm resolution, 3,600 points). In serial mapping, spectra are obtained sequentially from a series of positions using point-by-point scanning

978–1,178 cm^{-1} were used for investigating distribution of lignin and cellulose, respectively. A band range of 1,639–1,700 cm^{-1} was chosen for generating the image of coniferaldehyde and coniferyl alcohol distribution. For the double cell wall line scan, plots were generated using band regions of 309–399, 978–1,178, 1,519–1,712, and 2,773–3,045 cm^{-1} for the 380, 1,098, 1,600, and 2,900 cm^{-1} bands of cellulose and lignin, respectively. In these regions, integrated band intensity was calculated by the sloping baseline method. Spectral data and Raman images were not processed or manipulated in any way. Experimental error was close to 10%. This calculation was based on spectra obtained sequentially at different times from the same sample location.

Results and discussion

In the Raman spectrum of black spruce wood, contributions of cellulose, lignin and hemicelluloses have been identified (Agarwal and Ralph 1997) and the spectral features for both cellulose and lignin have been assigned (Agarwal 1999; Wiley and Atalla 1987). Earlier Raman studies both visible- and near-IR-excited (Agarwal and Atalla 1986, Atalla and Agarwal 1985; Bond and Atalla 1999; Tirumalai et al. 1996) of black spruce wood have indicated that spectral contributions of cellulose and lignin are detected in regions that, for the most part, do not overlap. However, the contribution of hemicelluloses was found to be weak, broad, and masked by the bands of cellulose due to the fact that hemicellulose bands are similar to cellulose bands and because hemicelluloses are non-crystalline. The non-crystallinity of hemicelluloses makes their Raman contributions broad and diffuse.

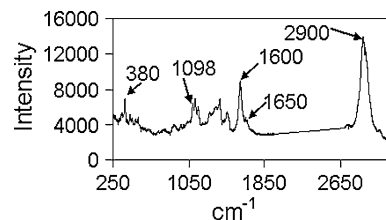


Fig. 3 Raman spectrum of S2 in transverse section of black spruce. Bands at 380, 1,098, and 2,900 cm^{-1} were due to cellulose. Lignin contributions were present at 1,600 and 1,650 cm^{-1} (Agarwal and Ralph 1997)

A Raman spectrum obtained from an S2 location in the cross section is shown in Fig. 3. The important bands of lignin and cellulose have been annotated. The band regions associated with these bands were used in generating the Raman images and the double cell wall line scan plots (described later).

Lignin band stability

As reported in earlier Raman microprobe work (Agarwal and Atalla 1986; Atalla and Agarwal 1985; Bond and Atalla 1999; Tirumalai et al. 1996), the 1,600 cm^{-1} band of lignin showed some decline when woody tissue was sampled in water and exposed to an intense laser beam (514.5 and 647 nm excitations). Although “water sampling” was not used here, it was considered prudent to check for any 1,600 cm^{-1} band instability. This was done by obtaining a series of sequential spectra from the same location in both S2 secondary wall and cell corner (CC) regions. The results for the S2 location are shown in Fig. 4, where the integrated band intensity is plotted against time. The plotted data in Fig. 4 clearly indicate that the band intensity remained constant (within experimental error, 16% for this experiment). An analysis of variance (ANOVA) indicated that that at the 95% confidence level, the linear regression model is not statistically

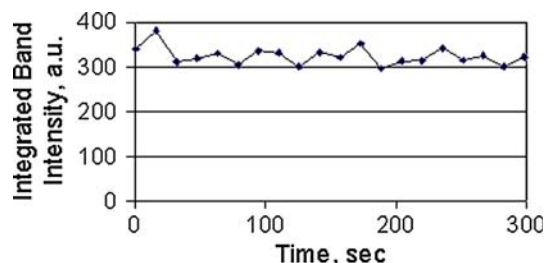


Fig. 4 Change in area intensity of 1,600 cm^{-1} band with time. Sampled spot was located in S2 layer and had not been previously exposed to the laser beam. Each point represents a 15-s acquisition

better than assuming that the data are constant. Similar results were obtained from the CC location.

Raman intensity versus analyte concentration

Raman band intensity I for an isotropic sample can be expressed as follows:

$$I = K\nu^4\sigma I_0 \exp\left(\frac{-E_i}{kT}\right) C_a V \quad (1)$$

where K is a constant, ν is absolute frequency of Raman band, σ is Raman cross section, I_0 is laser radiation intensity, $\exp(-E_i/kT)$ is Boltzmann factor for state i , (E_i is the energy for state i and T is temperature), C_a is analyte concentration, and V is sample volume illuminated by laser and viewed by Raman spectrometer. Although the band intensity in Eq. 1 depends on a number of factors, for a given instrument when samples are analyzed in a fixed geometry and at constant laser intensity I_0 , Eq. 1 reduces to a much simpler form:

$$I = K'VC_a \cdot \psi \quad (2) \leftarrow$$

In Eq. 2, K' is a new constant for each band or wavenumber interval. In addition, in a confocal mode when the sample surface is analyzed, the sample volume illuminated by the laser light and viewed by the Raman microscope can be considered to remain constant. In this case, Eq. 2 further reduces to

$$I = K''C_a \quad (3) \leftarrow$$

indicating that band intensity in Raman is directly proportional to concentration and quantitative measurements can be made as long as the assumptions underlying Eq. 3 remain fulfilled. These conditions were met in the present investigation, and Raman intensities associated with lignin and cellulose bands can be taken as indicators of their concentrations. Any effect of molecular orientation was assumed to be small and was ignored as a first approximation. For the lignin band at $1,600\text{ cm}^{-1}$, this is supported by previous work in which lignin orientation in the S2 transverse section produced less than a 20% change in Raman band intensity when the cell wall was parallel to the laser electric vector as opposed to perpendicular. In contrast, cellulose orientation in S2 was mostly perpendicular to the transverse plane and the $1,098\text{ cm}^{-1}$ band intensities were similar in both orientations. A future study is intended to explore the influence of lignin and cellulose cell wall orientation on Raman band intensity.

Latewood cell region

An annual ring in wood consists of a layer of cells produced in any 1 year and contains both earlywood and latewood cells (Sjostrom 1993). Latewood cell walls are thicker compared to earlywood cell walls because they are formed during the season when growth is slow. Within the cross section, a 30-by $30\text{-}\mu\text{m}^2$ region containing six latewood cells (Fig. 5) was selected for Raman mapping. This rectangular enclosed area contained three CCs and multiple mL, P, S1, S2, and S3 regions. The area was mapped at $0.5\text{-}\mu\text{m}$ x, y resolution, and 3600 spectra each for the lignin and cellulose regions were obtained to generate the Raman images. Figure 6 shows two- and three-dimensional Raman images of lignin distribution. These images are based on the integrated intensity of the wavenumber interval region that includes both the $1,600$ and $1,650\text{ cm}^{-1}$ bands of lignin. Although nine latewood areas (between 30th and 40th annual ring segments) similar to Fig. 5 have been investigated in the author's laboratory, in view of the similar results the data are discussed in detail from only one such latewood ring area.

Lignin distribution

In the Raman spectrum of black spruce, the most intense contribution from lignin was seen at $1,600\text{ cm}^{-1}$ (Fig. 3). The other main lignin feature was detected at $1,650\text{ cm}^{-1}$, due to the coniferaldehyde and coniferyl alcohol units (Agarwal 1999). Raman images of lignin

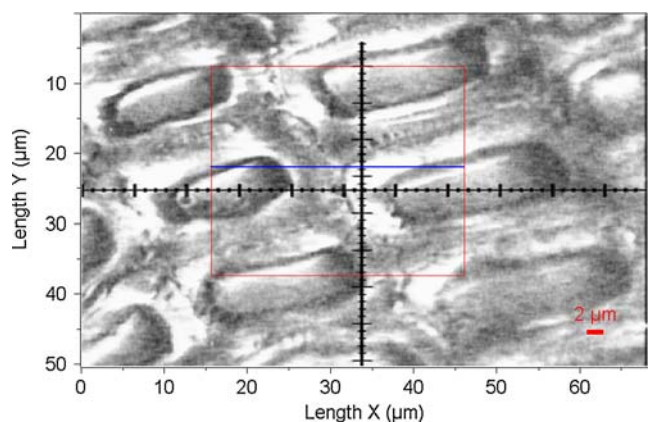


Fig. 5 Bright field image of spruce cross section (micrometer scale superimposed) showing selected area (red rectangle) for Raman mapping. Rectangle encloses cell walls of six adjoining mature tracheid cells and contains three CC regions. Raman images of this area are shown in Fig. 6 (lignin) and Fig. 9 (cellulose). A Y-segment at $Y = 21.6\text{ }\mu\text{m}$, for which results are discussed later, is marked in blue

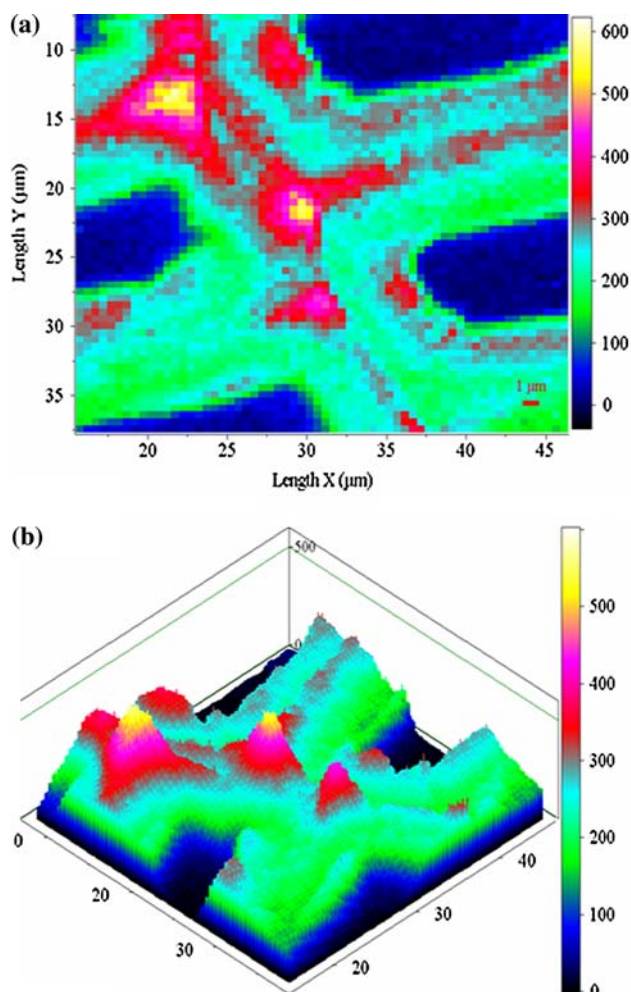


Fig. 6 Raman images (false color) of lignin spatial distribution in selected cell wall area in Fig. 5 in two-dimensional (a) and three-dimensional (b) representations. Intensity scale appears on the right. *Bright white/yellow* locations indicate high concentration of lignin; *dark blue/black* regions indicate very low concentration, e.g., lumen area

distribution were generated in two ways: using only the $1,600\text{ cm}^{-1}$ band (not reported here) and using both the $1,600$ and $1,650\text{ cm}^{-1}$ bands (Fig. 6). The $1,650\text{ cm}^{-1}$ contribution was included not only because it is a lignin feature but also because of its partial overlap with the band at $1,600\text{ cm}^{-1}$. However, the Raman images generated in these two different ways were almost identical, with the exception that the signal-to-noise ratio was slightly better for the two-band case. Therefore, we decided that the Raman images of lignin distribution would be generated using the combined band region of $1,519\text{--}1,712\text{ cm}^{-1}$. Figure 6a shows an image of the selected area in Figs. 5 and 6b is a three-dimensional representation of the distribution shown in Fig. 6a.

In the Raman image plots (Fig. 6), lignin concentration was highest (white/yellow, 600–500 counts) in

areas that correspond to CC (Fig. 5). In Fig. 5, three distinct CC areas were located in the selected area, but only two of those areas showed such a high lignin concentration. The third region ($x, y = 30.7, 28.5\text{ }\mu\text{m}$) had the next lower lignin concentration (magenta, ~ 425 counts). This lignin concentration was also found in areas that formed the outside cores of the first two CC areas (Fig. 6). The next level of intensity (red, 400–300 counts) was evident in not only the outer layers of all three CC regions but also in several spots located in CmL, in the S2 and S2–S3 areas. On the contrary, lignin concentration was much lower in numerous other mapped locations in these regions. This suggests that lignin concentration in a distinct morphological region is not uniform and varies significantly. In the top right cell shown in Fig. 6a, lignin concentration was high near the lumen (S2–S3 area), declined to a minimum in S2 near the CmL area (outer S2), and rose in the CmL area. But this pattern was not repeated in the other cells shown in Fig. 6a. In the lower right cell (Fig. 6a), lignin concentration depended on whether the S2–S3 region was in the top or bottom area of the cell wall. Lignin concentration was higher in the bottom compared to the top (Fig. 6a).

To compare spectra from various regions (CC, CmL, S2, S2–S3, and lumen), a set of spectra was extracted from the image in Fig. 6a and is shown in Fig. 7. Except for the lumen, all regions contained lignin bands at $1,600$ and $1,650\text{ cm}^{-1}$. Although not shown in Fig. 7, as noted previously, for any given morphological region the band intensity was location specific (Fig. 6a).

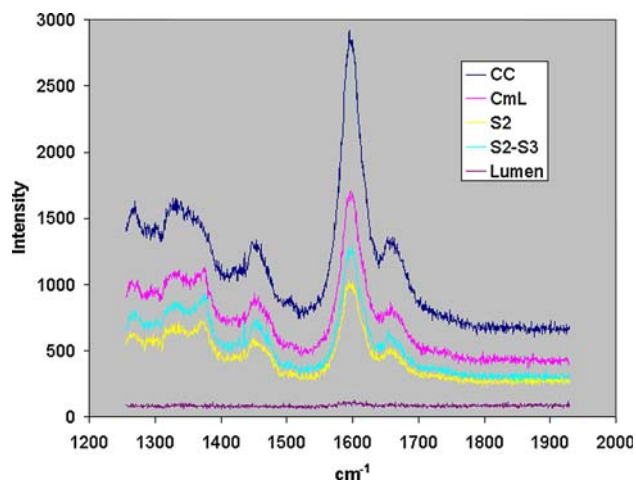


Fig. 7 Typical spectral bands of lignin from various cell wall regions. Higher lignin concentration is responsible not only for higher peaks at $1,600$ and $1,650\text{ cm}^{-1}$ but also for higher fluorescence background. Each spectrum represents individual location within a region. Spectral intensity within a region was location dependent (Fig. 6a)

Table 1 Comparison of CC-to-S2 lignin concentration ratio by different techniques

UV microscopy (Black spruce)	Br-EDXA, factor 1.7 ^a (Radiata pine)	Interferometry (Radiata pine)	Hg-EDXA (Norway spruce)	Raman imaging (Black spruce)
Latewood = 4.50 Earlywood = 3.77 Fergus et al. (1969)	X1 ^b _{avg} = 3.31 X2 _{avg} = 2.04 Donaldson (1992)	X1 ^b _{avg} = 3.39 X2 _{avg} = 4.23 Donaldson (1992)	Latewood = 2.52 Earlywood = 2.39 Westermarck et al. (1988)	Latewood < 2.4 ^c Present study

^aS2 lignin is 1.7 times more reactive compared to CC lignin; hence, a correction factor of 1.7 was taken into account

^b1 and 2 were matched samples (but sites were not matched)

^cEstimated

Therefore, for a particular region, band intensities were compared to get a sense of the range of variation in lignin concentration. Such comparisons indicated significant variation. For instance, within the S2 of the top right latewood cell (Figs. 5, 6a), lignin concentration varied by as much as 82%. The range of variation in lignin concentration for other regions was as follows: CC, 37%; CmL, 85%; S2–S3, 84%. For the S2 region, the range of variation was above and beyond what can be accounted for by the effect of orientation (20%), if present. Moreover, neighboring cell walls showed a similar pattern in variation of lignin concentration.

From the limited study conducted here, it appears that the variation in lignin concentration between identical cell wall regions of different cells is of a magnitude similar to the variation seen in a single cell region.

The finding that CC lignin concentration is non-uniform confirms our earlier Raman results for black spruce wood (Tirumalai et al. 1996). This variability in concentration can be explained by the reported existence (Daniel et al. 1991) of non-lignified and/or poorly lignified regions in CC areas smaller than 1 μm. Similarly, the heterogeneity of lignin distribution in S2 observed here provides support to findings published previously for different woods (Singh and Daniel 2001; Singh et al. 2002).

Considering that the lateral resolution of the confocal spot (~ 1 μm) is somewhat greater than the thickness of the CmL region (~ 0.7 μm) in Fig. 5, it is likely that CmL areas contained contribution from the S1 layers as well. Therefore, variation in the CmL region could arise from a number of cell wall layers: mL, P, and S1 layers. An even higher spatially resolved Raman microscope is needed to further discriminate between such contributions. Another observation concerns sampling at the lumen/S3–S2 interface. The lignin band was quite weak near the interface (Fig. 6), which was to be expected because the sampled spot at the interface contained some lumen.

As far as what else could be behind the variation in lignin band intensity in addition to composition, the

variation could be a reflection of lignin orientation; lignin orientation was previously detected for the S2 wall by Raman microscopy (Atalla and Agarwal 1985; Tirumalai et al. 1996). But considering that the effects of lignin orientation were reported to be small (less than 20%), this is unlikely to explain the variability range observed here for S2 (82%). Therefore, it is reasonable to assume that most variability in band intensity is due to changes in lignin concentration. We hope that a study specifically targeted at this aspect of the findings will reveal the extent to which variation in intensity can be interpreted in terms of orientation and concentration effects.

CC-to-S2 lignin concentration ratio

Using a number of techniques, the CC-to-S2 lignin concentration ratio has been reported for softwood fibers (Table 1). UV-microscopy data were found to be similar to Br-EDXA results, although a correction factor of 1.7 was needed to account for the difference in the reactivity of CC and S2 lignin (Saka and Thomas 1982). However, some Br-EDXA data have remained controversial. The data vary substantially and have been found to be site specific. Two additional methods, interferometry and Hg-EDXA, were developed for this purpose; the results are shown in Table 1. Previously, investigation of a limited area with Raman microscopy showed that the CC concentration of lignin was no more than twice that of the S2 in black spruce cross sections treated with sodium borohydride (Agarwal, Forest Products Laboratory, data on file). Many more S2 data were available for the present study, and the CC-to-S2 lignin concentration ratio can be calculated. For an average S2 lignin concentration of 250 intensity units (Fig. 6a) expressed as a ratio to the highest CC lignin concentration of 600 intensity units, the ratio is 2.4 (Table 1). This suggests that the CC-to-S2 lignin concentration ratio is unlikely to be higher than 2.4, but it can be lower because the CC concentration used in the calculation was the highest observed and was not an average value. As Table 1

indicates, the Raman imaging results support the results found by Hg-EDXA.

Coniferaldehyde and coniferyl alcohol distribution

Considering that the Raman band at $1,650\text{ cm}^{-1}$ (Fig. 3) is due to the coniferaldehyde and coniferyl alcohol (Agarwal 1999), two of the many substructures in lignin, their morphological distribution in the mapped area (Fig. 5) can be studied. For spruce, an earlier study (Peng and Westermark 1997) examined such a morphological distribution and found that, compared to S2, both P and S1 cell wall layers were enriched in both coniferaldehyde and coniferyl alcohol groups. The study also reported that the mL and S3 regions were enriched only in coniferyl alcohol. These results imply that if CmL is sampled, as is done in Raman mapping, enrichment would be expected as a result of both the aldehyde and alcohol structures. In addition, the S2–S3 region is expected to be more intense when an image is generated using the $1,650\text{ cm}^{-1}$ band. Figure 8 shows such an image of the area. However, the distribution in Fig. 8 was similar to that shown in Fig. 6a for lignin, and, contrary to expectation, no enrichment in the CmL or S2–S3 areas was detected.

Cellulose distribution

Two- and three-dimensional Raman images of cellulose distribution are shown in Fig. 9. For the S2 layer, cellulose distribution was much more uniform (mostly red/magenta, Fig. 9) compared to that of lignin. This

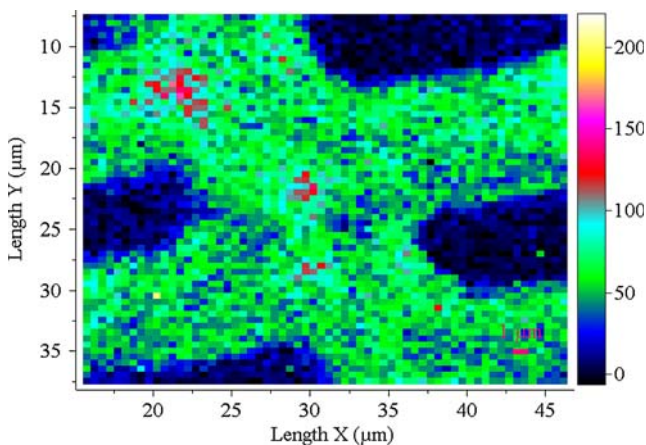


Fig. 8 Two-dimensional Raman image (false color) of spatial distribution of lignin coniferaldehyde and coniferyl alcohol units in area selected in Fig. 5. Intensity distribution pattern is similar to lignin distribution in Fig. 6a. *Bright white/yellow* locations indicate high concentration of coniferaldehyde and/or coniferyl alcohol units; *dark blue/black* regions indicate very low concentration, e.g., lumen area

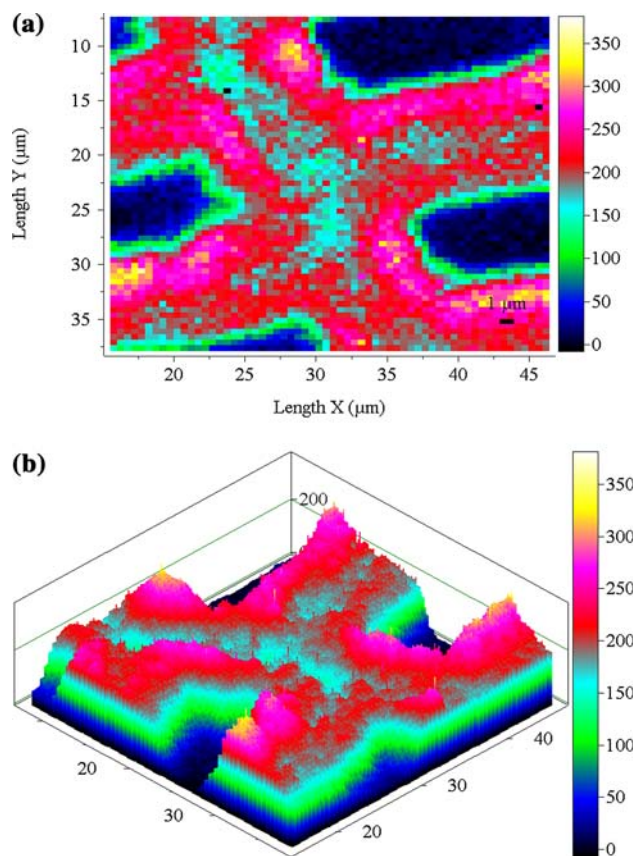


Fig. 9 Raman images (false color) of cellulose spatial distribution in cell wall area selected in Fig. 5; two-dimensional (a) and three-dimensional (b) representations. *Bright white/yellow* locations indicate high cellulose concentration; *dark blue/black* regions indicate very low concentration, e.g., lumen area

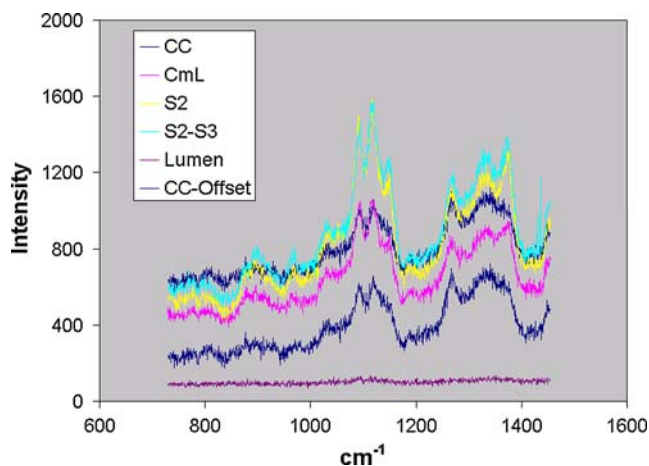


Fig. 10 Typical spectra in cellulose frequency range. Spectrum CC-Offset is same as CC but has been y-offset by 400 intensity units for better visualization. Higher cellulose concentration is responsible for higher peaks at $1,098$, $1,123$, and $1,150\text{ cm}^{-1}$. Each spectrum represents individual location within region; spectra from different locations within a region may vary in intensity

may reflect that in the S2, cellulose is oriented more or less parallel to the longitudinal axis of the cell and concentration variations within the S2 in the cross section will have only a weak impact on the intensity of the 978–1,178 cm^{-1} region. Nevertheless, there were few S2 and S2–S3 locations of high (white/yellow) cellulose concentration. Figure 9 also shows many locations where cellulose concentration was low (blue/green, 150–125 counts). The latter correspond to the CC and CmL regions of the tissue. All three CC areas behaved similarly in this regard. This is expected because regions of highest lignin concentration, that is, CCs, are known to be locations of low cellulose concentration (Burke et al. 1974; Meier 1985; Whiting and Goring 1983). High cellulose concentration (350–300 counts) spots were confined mostly to S2 and S2–S3 regions.

Considering that cellulose is a semicrystalline polymer and oriented differently in different layers, the variation in intensity between regions containing different wall layers is likely to be related to micro-fibril orientation. This aspect will be explored further in future studies that focus on the effect of orientation on band intensity. Here, the lumen/S3–S2 interface once again produced weak cellulose intensity (green/light blue region) because the mapped area at the interface consisted of some lumen.

To compare cellulose spectra from various cell regions (CC, CmL, S2, S2–S3, and lumen), a set of spectra that were extracted from different locations in the image in Fig. 9a are shown in Fig. 10. Although the cellulose bands in four of the five regions are similar in terms of spectral features and wavenumber positions, the spectrum belonging to the CC region (dark blue in Fig. 10) showed a significant difference. In addition to weak intensity, the features of this spectrum were broad and not well resolved. This was likely due to the disordered/amorphous nature of cellulose in the CC region. Moreover, for a given cell wall region, the band intensity varied (Fig. 9a) depending on the specific location in the region. This was true for both the S2 and the S2–S3 regions but less so for the CmL and the CC regions. Nevertheless, for a particular morphological region, intensities can be compared to get a notion of the range of variation in cellulose band intensity. Such comparisons provided further support that the cellulose concentration varied.

For instance, within the S2 region of the top right latewood cell in Fig. 5, cellulose intensity varied by as much as 33%, although intensity beyond this variation range was also detected in a few spots. Cellulose crystallinity, crystallite size, and mean fibril angle could all be the cause of this variability but these parameters have been reported to show only limited variation in

mature wood (Andersson et al. 2003; Newman 2004; Peura et al. 2005). Consequently, within the S2 layer, the intensity changes are likely to be a measure of differences in cellulose concentration.

On the other hand, interpretation of such changes in the S2–S3 region is more complex due to the fact that the S3 layer, compared with S2, has a different net orientation of cellulose chains. It has been reported that S3 has crossed lamellar structure (Imamura et al. 1972; Wardrop 1954), which is caused by both the presence of alternating right- and left-handed helices and also by the different orientation of the cellulose fibrils. However, considering that the thickness of the S3 layer is only 1/10 (0.1 μm) of the lateral resolution (1 μm), the S3 layer is likely to have a limited role and it can be assumed that the variation seen in the S2–S3 region is predominantly due to the S2 layer. For other regions, the range of cellulose concentration was 41% for CC, 63% for CmL, and 100% for S2–S3. Presently, intensity differences within and between regions cannot be explained on the basis of what is known about cell wall architecture. The Raman data seem to reflect the complexity of cellulose organization. In this respect, we hope that further studies, including those of longitudinal wood sections, will provide useful information.

Lignin and cellulose variation along selected y-segment

To visualize how lignin and cellulose concentration varied along the x dimension at a selected y -position, a y -segment that passed through the CC location was taken at $y = 21.6 \mu\text{m}$ (Fig. 5). The results are shown in Fig. 11a. As the various x -positions were sampled at this y -position, changes in intensity, in both lignin and cellulose, could be observed within and across different regions. Locations in S2 indicated that the lignin composition of most such spots produced 150–300 intensity units (Fig. 11a), implying that close to 100% variation occurred within the S2 of all cells (as mentioned previously, for the top right cell, S2 lignin concentration varied by as much as 82%). In the case of cellulose, although the CC area showed the lowest cellulose concentration of about 150 intensity units (Fig. 11a), most S2 areas had somewhat higher cellulose concentration (150–250 intensity units). In some places, lignin concentration seemed to follow cellulose concentration (Fig. 11a, left of center). Nevertheless, there are also areas that do not follow this trend (Fig. 11a, S2 right of center). The reason for this behavior remains unknown.

To visualize the deviation even better, lignin concentration along the segment points was divided by

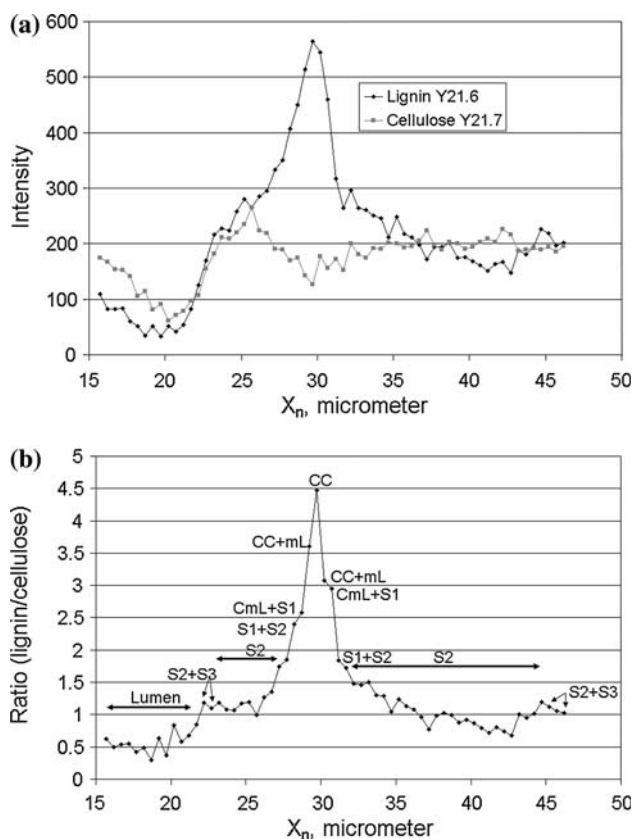


Fig. 11 Variation in lignin and cellulose concentrations. **a** Variation along x -dimension. Data sets for lignin ($y = 21.6 \mu\text{m}$) and cellulose ($y = 21.7 \mu\text{m}$) are essentially from same y -segment considering that lateral resolution ($1 \mu\text{m}$) is significantly larger than difference ($0.1 \mu\text{m}$) in y -segment positions. **b** Variation of lignin-to-cellulose ratio for $21.6 \mu\text{m}$ y segment

cellulose concentration; the result is shown in Fig. 11b. The impact of high lignin and low cellulose concentrations of CC is obvious. The other morphological regions showed smaller variation compared to the ratio of lignin to cellulose in the CC region. For several locations in the region around $x = 25 \mu\text{m}$, the ratio was constant and reflected the fact that at these locations the concentrations of both lignin and cellulose increased or declined simultaneously. Plots similar to those shown in Fig. 11 can be generated from various y - and/or x -segments, which can lead to a better appreciation of the variability and tendencies of lignin and cellulose concentrations in various parts of the cell wall.

Double cell wall line scan

A double cell wall line scan (Fig. 12a) was carried out using four Raman band regions (380 , $1,098$, $1,600$, and $2,900 \text{ cm}^{-1}$). In addition to obtaining information on how cellulose and lignin concentrations vary across the neighboring cell walls, our intent was to discover any

differences among the plots generated using the different bands of cellulose (380 , $1,098$, and $2,900 \text{ cm}^{-1}$). A $13.7\text{-}\mu\text{m}$ -long line scan was carried out in the y -direction with a y spatial resolution of $0.1 \mu\text{m}$. The reason for such a high y resolution was to see if areas of sudden concentration change, if any, could be identified near the CmL region. Considering that the lateral resolution of the Raman probe is significantly larger than the true mL width, this approach was thought to be one possible way to delineate concentration differences. All the cellulose band profiles showed a similar pattern (Fig. 12b), although signal-to-noise was greatly enhanced in the $2,900 \text{ cm}^{-1}$ plot. This was due to the fact that the $2,900 \text{ cm}^{-1}$ Raman band is the most intense band in the spectrum of the transverse section (Fig. 3). The similarity of the three band profiles indicated that any small contribution by lignin in the spectral regions of the $1,098$ and $2,900 \text{ cm}^{-1}$ band profiles did not distort the results to any significant degree. Note that of these three spectral regions, only the 380 cm^{-1} band region ($309\text{--}399 \text{ cm}^{-1}$) had contribution from cellulose alone; the other two band regions, $1,098$ and $2,900 \text{ cm}^{-1}$ ($978\text{--}1,178$ and $2,773\text{--}3,045 \text{ cm}^{-1}$, respectively) had definite but small contributions from lignin and/or other hemicelluloses

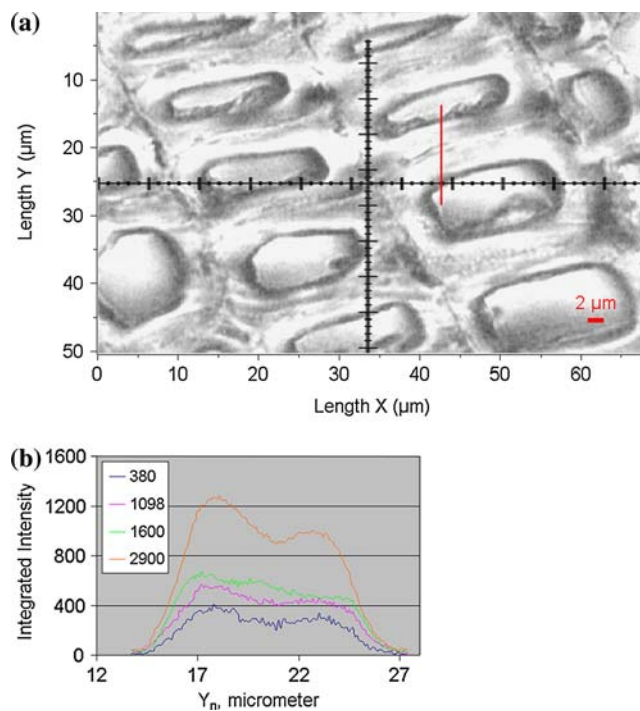


Fig. 12 Double cell wall line scan: **a** Bright field image of spruce cross section showing line scan (red) in y -direction. From the $13.7\text{-}\mu\text{m}$ -long scan, 138 spectra in each spectral region were obtained; **b** Raman intensity variation in each spectral region—lignin ($1,600$) and cellulose (380 , $1,098$, and $2,900$)

(Agarwal and Ralph 1997). The advantage of using only one cellulose region is to reduce experiment time; if the $2,900\text{ cm}^{-1}$ region is used, the additional advantage is higher signal-to-noise in the images. The latter translates to more confidence in the analysis. On the basis of these findings, for cellulose, results from the $2,900\text{ cm}^{-1}$ region were considered better than those from the 380 and $1,098\text{ cm}^{-1}$ regions.

As the scan moved from the top lumen (Fig. 12a) to the lower lumen, it detected a rise in cellulose concentration in S2, a gradual decline to a minimum value in CmL, another rise to a high value in the S2 region of the lower cell wall, and finally a drop in concentration in the lower lumen (Fig. 12b). We do not know why the bands showed a slightly higher maximum intensity on the left side of the plot. This phenomenon could be real or a feature associated with the experiment. For instance, it is possible that underlying fluorescence played a role, although intensity was calculated using the base-line method. It is known that woody tissue fluorescence decays with time. By the time the lower cell wall was sampled, the latter area had been exposed to the diffuse 633-nm light for quite some time. Any contribution of residual fluorescence to band intensity is bound to be lower than the contribution from the upper cell wall. However, such behavior was not observed in the x, y maps (Figs. 6, 9). Another possibility could be the unevenness of the microtomed wood section. Micron level roughness is expected when wood is microtomed.

The lignin intensity profile ($1,600\text{ cm}^{-1}$ curve in Fig. 12b) showed an additional peak in the center of the curve. In addition, compared to the cellulose profiles, the lignin profile is broader on the S3 side, indicating high lignin concentration in both S2 and S3. Lignin concentration declined somewhat toward the CmL area, increased somewhat, and then slightly declined again. As the scan continued into the lower cell wall, lignin intensity rose again in S2 and S3, prior to falling monotonically as the scan moved towards the lumen. Contrary to expectation, no significant intensity enhancement in the CmL region that was not already present in S2 and S3 was seen in the double cell wall scan. This result may be related to laser spot size or to the fact that this is an mL region with low lignin concentration (note similar areas in Fig. 6).

Lignin-to-cellulose ratio

The ratio of lignin to cellulose concentration is plotted in Fig. 13. Three plots were generated for three bands of cellulose (380 , $1,098$, and $2,900\text{ cm}^{-1}$). The signal-to-noise varied between the plots and, as expected, was

lower for the $1,600/380$ plot (Fig. 13) due to the low intensity of the 380 cm^{-1} band. Nevertheless, all three bands showed a similar pattern in regard to variation in the value of the ratio across the double cell wall. When variation in lignin and cellulose concentration is taken into account (Fig. 12b), it is clear that lignin concentration in the CmL and S2–S3 regions was significantly higher than that in most of the S2 region. This implies that the CmL and S2–S3 regions of the cell wall are enriched in lignin. Although the CmL result was expected based on the known higher concentration of mL areas, the greater lignification of S2–S3 is not well established. This finding lends further support to the mapping results in Fig. 6a, where lignin concentration was indeed higher in many S2–S3 areas compared with S2.

Future directions

This study indicates that Raman imaging methodology is a very useful tool for analyzing plant cell walls without the use of stain, dye, and contrast agent. Because of its unique spectral capability, this technique provides component-specific spatially resolved information in intact biological tissue, so that no sample preparation other than microtoming is required. Furthermore, this technique allows the correlation of chemical and morphological information. In the future, Raman images are likely to be analyzed in conjunction with contemporary data analysis tools like chemometrics (e.g., principal component analysis) and multivariate curve resolution to obtain detailed information on cell wall organization and interactions between cell

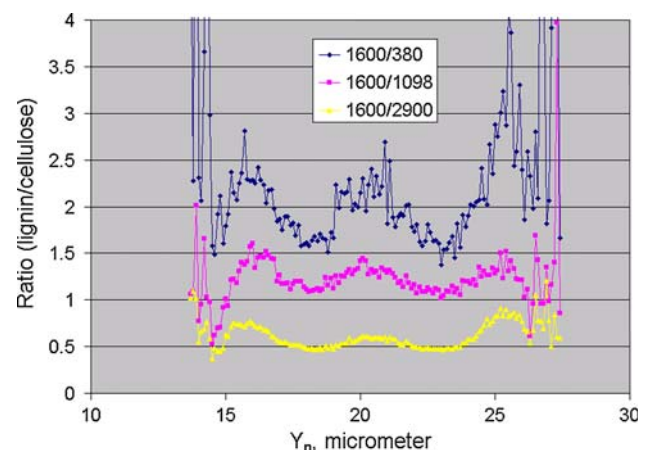


Fig. 13 Variation of lignin-to-cellulose concentration ratio across double cell wall. Compared with concentration in most of S2, concentration in CmL and S2–S3 regions showed significant enhancement. The y -sampling was conducted in $0.1\text{-}\mu\text{m}$ steps

wall components. Moreover, since Raman imaging permits optical sectioning and imaging in three dimensions, it is expected that this capability will be exploited to generate even more useful insights.

The present effort is directed toward generating normal or baseline compositional information on the wood cell wall to help answer the question of what constitutes a normal wood cell wall. The fundamental information generated will affect a number of research areas including the modeling of the plant cell wall. Although numerous areas will benefit from the currently demonstrated advance, study of chemically and biologically processed samples wherein differences due to process chemistry can be elucidated would certainly be an area worth investigating. This fundamental research capability to characterize plant cell walls in situ has potential not only to advance the structural and functional understanding of cell walls but, in the long term, to contribute towards better utilization of biomaterials.

Conclusions

Confocal Raman microscopy was successfully used to generate images of lignin and cellulose distribution in black spruce latewood cell walls. The Raman images indicated that at the microscopic level the concentrations of both lignin and cellulose varied both within and between distinct morphological regions. Whereas CC lignin concentration was the highest on average, lignin concentration in CmL was not all that different from that in S2 and S2–S3. In contrast, cellulose distribution, for the most part, showed an opposite pattern. For a particular cell wall region, the magnitude of variability in concentration was similar within and between neighboring wood cells. Based on the variability seen in the contributions of lignin and cellulose, the macromolecular organization of the wood cell wall is quite complex.

Acknowledgements The author thanks the following staff of the Forest Products Laboratory for their contributions to this work: Karen Berton, preparation of Fig. 1; Tom Kuster, preparation of microtomed sections; and Jim Beecher and Carl Houtman, helpful comments on the draft of the manuscript.

References

- Agarwal UP (1999) An overview of Raman spectroscopy as applied to lignocellulosic materials. In: Argyropoulos E (ed) *Advances in lignocellulosics characterization*, Ch. 9. TAPPI Press, Atlanta, pp 201–225
- Agarwal UP, Atalla RH (1986) In-situ Raman microprobe studies of plant cell walls: macromolecular organization and compositional variability in the secondary wall of *Picea mariana* (Mill.) B.S.P. *Planta* 169:325–332
- Agarwal UP, Ralph SA (1997) FT-Raman spectroscopy of wood: identifying contributions of lignin and carbohydrate polymers in the spectrum of black spruce. *Appl Spectro* 51:1648–1655
- Åkerholm M, Salmén L (2003) The oriented structure of lignin and its viscoelastic properties studied by static and dynamic FT-IR spectroscopy. *Holzforschung* 57:459–465
- Andersson S, Serimaa R, Paakkari T, Saranpää P, Pesonen E (2003) Crystallinity of wood and size of cellulose crystallites in Norway spruce (*Picea abies*). *J Wood Sci* 49:531–537
- Atalla RH, Agarwal UP (1985) Raman microprobe evidence for lignin orientation in the cell walls of native woody tissue. *Science* 227:636–638
- Baldwin KJ, Batchelder DN, Webster S (2002) Raman microscopy: confocal and scanning near-field. In: Lewis IR, Edwards HG (eds) *Handbook of Raman spectroscopy*, Ch. 4. Marcel Dekker Inc, New York, pp 145–190
- Bond JS, Atalla RH (1999) A Raman microprobe investigation of the molecular architecture of loblolly pine tracheids. In: *Proceedings of 10th international symposium on wood pulp chemistry*, vol 1. TAPPI Press, Atlanta, pp 96–101
- Bradbury S (1989) *An introduction to the optical microscope*. Oxford University Press, New York, p 29
- Burke D, Kaufman P, McNeil M, Albersheim P (1974) The structure of plant cell walls: VI. A survey of the walls of suspension-cultured monocots. *Plant Physiol* 54:109–115
- Daniel G, Nilsson T, Pettersson B (1991) Poorly and non-lignified regions in the middle lamella cell corners of birch (*Betula verrucosa*) and other wood species. *IAWA Bull* 12:70–84
- Donaldson LA (1992) Interference microscopy. In: Lin SY, Dence CW (eds) *Methods in lignin chemistry*, Ch. 4. Springer, Berlin Heidelberg New York, pp 122–132
- Donaldson LA, Ryan KG (1987) A comparison of relative lignin concentration as determined by interference microscopy and bromination/EDXA. *Wood Sci Technol* 21:303–309
- Ehrnrooth EML, Kolseth P, de Ruvo A (1984) The influence of softening and lignin removal on the mechanical-behavior of wood pulp fibers. *Svensk Papperst* 12:R78–R82
- Eriksson I, Lidbrandt O, Westermark U (1988) Lignin distribution in birch (*Betula verrucosa*) as determined by mercurization with SEM- and TEM-EDXA. *Wood Sci Technol* 22:251–257
- Fengel D, Wegner G (1984) *Wood—chemistry, ultrastructure, reactions*, Ch 3. Walter de Gruyter, Berlin, pp 26–65
- Fergus BJ, Procter AR, Scott JAN, Goring DAI (1969) The distribution of lignin in sprucewood as determined by ultraviolet microscopy. *Wood Sci Technol* 3:117–138
- Green DW, Winandy JE, Kretschmann DE (1999) Mechanical properties of wood. In: *Wood handbook*, FPL-GTR-113. U.S. Department of Agriculture, Forest Service, Forest Products Laboratory, Madison
- Imai T, Terashima N (1992) Determination of the distribution and reaction of polysaccharides in wood cell walls by the isotope tracer technique. IV. Selective radio-labeling of xylan in magnolia (*Magnolia kobus*) and visualization of its distribution in differentiating xylem by microautoradiography. *Mokuzai Gakkaishi* 38:693–699
- Imamura Y, Harada H, Saiki H (1972) Electron microscopic study on the formation and organization of the cell wall in coniferous tracheids—Crisscrossed and transition structures in the secondary wall. *Bull Kyoto Univ Forestry* 44:183–193
- Meier H (1985) Localization of polysaccharides in wood cell walls. In: Higuchi T (ed) *Biosynthesis and biodegradation of wood components*. Academic, Orlando, Florida, pp 43–50

- Newman RH (2004) Homogeneity in cellulose crystallinity between samples of *Pinus radiata* wood. *Holzforschung* 58:91–96
- Olsson A-M, Salmén L (1997) The effect of lignin composition on the viscoelastic properties of wood. *Nord Pulp Paper Res J* 12:140–144
- Parameswaran N, Liese W (1982) Ultrastructural localization of wall components in wood cells. *Holz roh Werkst* 40:145–148
- Peng F, Westermark U (1997) Distribution of coniferyl alcohol and coniferaldehyde groups in the cell wall of spruce fibres. *Holzforschung* 51:531–536
- Puera M, Müller M, Serimaa R, Vainio U, Sarén M-P, Saranpää P, Burghammer M (2005) Structural studies of single wood cell walls by synchrotron X-ray microdiffraction and polarized light microscopy. *Nucl Inst And Meth B* 238:16–20
- Roder T, Koch G, Sixta H (2004) Application of confocal Raman spectroscopy for the topochemical distribution of lignin and cellulose in plant cell walls of beech wood (*Fagus sylvatica* L.) compared to UV microspectrophotometry. *Holzforschung* 58:480–482
- Saka S, Goring DAI (1988) Distribution of lignin in white birch wood as determined by bromination with TEM-EDXA. *Holzforschung* 42:149–153
- Saka S, Thomas RJ (1982) Evaluation of the quantitative assay of lignin distribution by SEM-EDXA-technique. *Wood Sci Technol* 16:1–18
- Salmén L, Olsson A-M (1998) Interaction between hemicellulose, lignin, and cellulose: structure, property relationships. *J Pulp Paper Sci* 24:99–103
- Scott JAN, Procter AR, Fergus BJ, Goring DAI (1969) The application of ultraviolet microscopy to the distribution of lignin in wood description and validity of the technique. *Wood Sci Technol* 3:73–92
- Singh AP, Daniel G (2001) The S₂ layer in the tracheid walls of *Picea abies* wood: Inhomogeneity in lignin distribution and cell wall microstructure. *Holzforschung* 55:373–378
- Singh AP, Daniel G, Nillson TJ (2002) Ultrastructure of the S₂ layer in relation to lignin distribution in *Pinus radiata* tracheids. *Wood Sci* 48:95–98
- Sjostrom E (1993) Wood chemistry. Fundamentals and applications, 2nd edn, Ch 1. Academic, San Diego, pp 1–20
- Tirumalai VC, Agarwal UP, Obst JRO (1996) Heterogeneity of lignin concentration in cell corner middle lamella of white birch and black spruce. *Wood Sci Technol* 30:99–104
- Wardrop AB (1954) Observations on crossed lamellar structures in the cell walls of higher plants. *Austral J Bot* 2:154–164
- Westermark U, Lidbrandt O, Eriksson I (1988) Lignin distribution in spruce (*Picea abies*) determined by mercurization with SEM-EDXA technique. *Wood Sci Technol* 22:243–250
- Whiting P, Goring DAI (1983) The composition of carbohydrates in the middle lamella and secondary wall of tracheids from black spruce wood. *Can J Chem* 61:506–508
- Wiley JH, Atalla RH (1987) Band assignments in the Raman spectra of celluloses. *Carbohydrate Res* 160:113–129